

# 000 001 002 003 004 005 Dejavu: Post-Deployment Learning for Embodied Agents 006 via Experience Feedback 007 008 009

010 **Anonymous authors**  
011 Paper under double-blind review  
012  
013  
014  
015  
016  
017  
018  
019  
020  
021  
022  
023  
024  
025  
026

## 027 Abstract 028

029 Embodied agents face a fundamental limitation: once deployed in real-world  
030 environments to perform specific tasks, they are unable to acquire new useful  
031 knowledge to enhance task performance. In this paper, we propose a general  
032 post-deployment learning framework called Dejavu, which employs an Experience  
033 Feedback Network (EFN) and augments the frozen Vision-Language-Action  
034 (VLA) policy with retrieved execution memories. EFN automatically identifies  
035 the most contextually successful prior action experiences and conditions action  
036 prediction on this retrieved guidance. We adopt reinforcement learning with  
037 semantic similarity rewards on EFN to ensure that the predicted actions align with  
038 past successful behaviors under current observations. During deployment, EFN  
039 continually enriches its memory with new trajectories, enabling the agent to ex-  
040 hibit “learning from experience” despite fixed weights. Experiments across di-  
041 verse embodied tasks show that EFN significantly improves adaptability, robust-  
042 ness, and success rates over frozen baselines. These results highlight a promis-  
043 ing path toward embodied agents that continually refine their behavior after de-  
044 ployment. We provide the code and demo on our anonymous website <https://dejavu2025.github.io/>.  
045  
046

## 047 1 Introduction 048

049 Embodied intelligence is an emerging paradigm in artificial intelligence, wherein an agent learns and  
050 makes decisions through physical interaction with environment (Liu et al., 2025a; Wang et al., 2024).  
051 Recently, unified Vision-Language-Action (VLA) models have achieved remarkable generalization  
052 across diverse tasks (Zitkovich et al., 2023; Shao et al., 2025; Firoozi et al., 2025; Han et al., 2026).  
053 However, these capabilities come at the cost of relying entirely on massive offline training with a  
054 fixed, unified dataset distribution (Brohan et al., 2023; Ha et al., 2024). Once deployed, the model’s  
055 weights (and thus its knowledge) remain fixed, which will not be updated without retraining (Liu  
056 et al., 2024a). Indeed, while users might expect an AI robot to continue learning from new situations,  
057 the reality is that most deployed models “stop learning” upon deployment (Liu et al., 2024a).  
058

059 Given this limitation, we naturally ask: do intelligent systems always need to rewrite their internal  
060 weights to improve? Humans, for instance, often tackle new problems not by learning entirely  
061 new facts, but by recalling relevant past experiences and reusing them (Andrychowicz et al., 2017;  
062 Oh et al., 2018). For example, an auto mechanic might fix a new engine issue by remembering a  
063 similar fault in another car and copying that solution. This ability to draw on episodic memories,  
064 which gives rise to the sense of “déjà vu” from having seen something similar before, does not alter  
065 core knowledge representations, yet it enables fast adaptation to new challenges by analogy to  
066 past experiences (Goyal et al., 2022). Inspired by this intuition, we ask: can an AI agent improve  
067 itself by recalling and reusing its “experiences” in a similar way? If a neural network could leverage  
068 stored memories of situations and solutions to inform its current decision-making, effectively  
069 learning from its own experience at inference time, then even a fixed-weight model could become  
070 better over time (Goyal et al., 2022). Such an agent would gain the ability to improve performance  
071 post-deployment, simply by accumulating and drawing upon new experiences, without any gradient-  
072 based re-training (Behrouz et al., 2024; Wang et al., 2025; Bagatella et al., 2025). This intriguing  
073 concept, which we term “learning from déj  vu”, motivates our approach.  
074

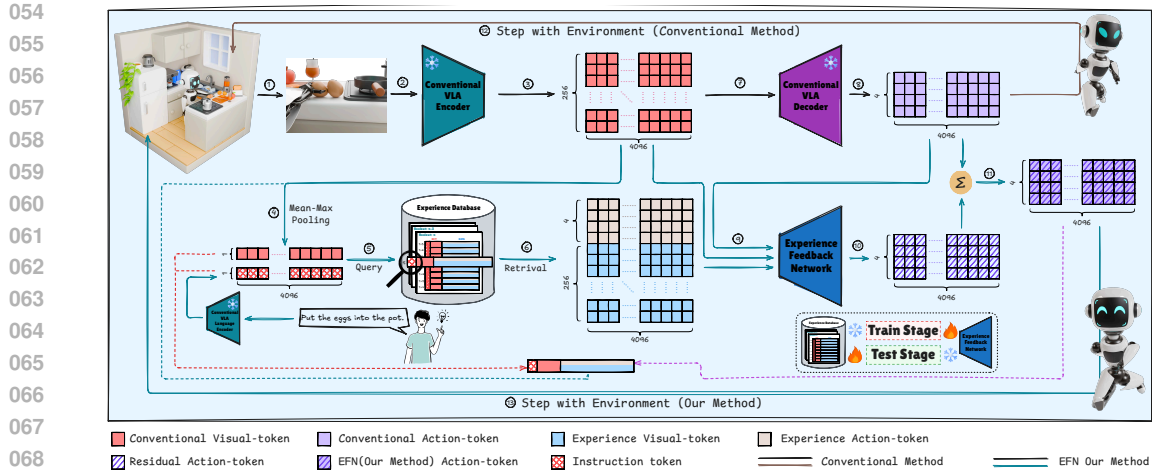


Figure 1: Top: a policy is trained once and then deployed with frozen weights, which prevents adaptation at test time. Bottom: a frozen VLA policy is augmented by an Experience Feedback Network that retrieves semantically relevant prior trajectories, produces residual corrections, and closes the loop with outcome similarity signals while keeping the base policy unchanged.

To realize this idea, we organize the design around four questions. *What is an experience, and in what format?* We define an experience as a trajectory of synchronized vision, language, and action; each rollout is stored in an experience bank aligned with the VLA interface. *How is experience reused?* We learn a network that takes the current observation together with a retrieved experience and predicts a **residual action**, which is added to the base policy’s output to form the final action (Johannink et al., 2019; Liu et al., 2025b). *How is the experience matched?* Because real-world perception is dominated by vision and language, we retrieve the most relevant trajectory using language-conditioned visual similarity. *How is such a network trained?* We optimize it with reinforcement signals shaped by a dense similarity between the predicted next observation and the next state in the retrieved trajectory, enabling effective assignment while keeping the backbone frozen.

Bringing these ideas together, we introduce the Experience Feedback Network (EFN). EFN takes the current observation and an action retrieved from a matched experience, and predicts a residual action. This residual is added to the VLA policy’s baseline output to produce the final control, which is then executed to yield the next observation. The intuition is straightforward: when a strong prior experience exists, EFN should exploit it to refine the action. We therefore train EFN with reinforcement learning using a dense, similarity-based reward: if the next observation resembles the *next observation in the retrieved experience*, the agent receives a higher reward, indicating that it is moving closer to that experience. This design supplies frequent shaping signals, unlike sparse success–failure rewards, and thus eases optimization. We optimize EFN with the soft actor–critic algorithm, which provides entropy regularization for robust exploration, stable value learning, and off-policy sample efficiency that enables effective reuse of stored experiences (Haarnoja et al., 2018).

During deployment, we maintain a *live* experience bank that is continuously augmented with newly successful rollouts. At every inference step, the agent retrieves similar trajectory in a joint vision–language embedding space and feeds the matched experience action to EFN alongside the current observation. EFN then predicts a residual action that refines the base VLA output as the final control. We integrate EFN with OpenVLA (Kim et al., 2024), UniVLA (Bu et al., 2025b), and the recent GO-1 (Bu et al., 2025a), and evaluate in both simulation and the real world: LIBERO for simulated tasks and the AgiBot G1 robot for physical experiments (Liu et al., 2023; Pumacay et al., 2024). Across all settings, EFN improves deployment-time performance over the base policies. We summarize our main contributions as follows:

- We introduce EFN as an *experience-centric* deployment-time mechanism that couples a live *experience bank* with a lightweight controller to improve VLA policies. By training such a network, the model can still *learn from experience* after deployment.
- We formalize an *experience* as a synchronized vision–language–action trajectory and retrieve candidates in a joint vision–language space; the retrieved step provides a matched *action prior* and its successor frame as the semantic target for guidance.

- 108 • We integrate EFN with OpenVLA, UniVLA, and GO-1, demonstrating consistent deployment-  
 109 time improvements on both simulation tasks and real-world platform.  
 110

111 **2 Background**  
 112

113 **2.1 Vision–Language–Action (VLA) Models**  
 114

115 Large-scale VLA policies have rapidly advanced the coupling of open-vocabulary perception with  
 116 end-to-end control (Shukor et al., 2025; Zhang et al., 2025; Zhai et al., 2025; Cheang et al., 2025).  
 117 The Robotics Transformer family established that scaling data and model capacity yields substantial  
 118 cross-task generalization in real-world manipulation (Brohan et al., 2023; Zitkovich et al., 2023).  
 119 Building on this, open-source generalist policies trained on heterogeneous, multi-robot corpora  
 120 demonstrated practical adaptation to new sensors and action spaces with modest finetuning, im-  
 121 proving accessibility and reproducibility for the community (Ha et al., 2024; Kim et al., 2024).

122 Recent architectures emphasize *efficiency* without sacrificing reasoning ability: state-space–inspired  
 123 designs reduce inference cost while preserving long-horizon context, enabling deployment on  
 124 resource-constrained platforms (Liu et al., 2024b). In parallel, standardized benchmarks for compo-  
 125 sitional generalization and knowledge transfer provide clearer axes to evaluate scale, robustness, and  
 126 post-deployment behavior of VLA policies (Liu et al., 2023). These developments position VLAs  
 127 as strong frozen backbones that can be *augmented at inference time*—a setting where our experience  
 128 feedback mechanism refines actions using retrieved trajectories without retraining the base model.  
 129

130 **2.2 Post-deployment Learning and Our Perspective**  
 131

132 A central challenge in deploying robotic policies is *improving competence after deployment* without  
 133 retraining. Human-in-the-loop frameworks study how robots can collect corrective signals and up-  
 134 date behavior during real operations, showing that runtime monitoring and continual data collection  
 135 can safely enhance autonomy in the field (Liu et al., 2024a). A complementary thread reduces the  
 136 burden on parametric updates by exploiting *retrieval at inference time*: retrieval-augmented rein-  
 137 forcement learning conditions decision-making on relevant past trajectories, so the agent can lever-  
 138 age experience without immediately folding it into weights (Goyal et al., 2022; Toteja et al., 2025;  
 139 Bacciu et al., 2023; Tarasov et al., 2025). Orthogonal to retrieval, *residual policy* improves a strong  
 140 but imperfect controller by predicting an additive correction, enabling faster adaptation than learning  
 141 a policy from scratch (Johannink et al., 2019). Finally, benchmarks for *lifelong and continual robot*  
 142 *learning* provide axes to quantify transfer, robustness, and knowledge accumulation across tasks,  
 143 highlighting the need for systematic evaluation of post-deployment behavior (Liu et al., 2023).

144 **Our differences.** As shown in 1, EFN targets the post-deployment setting and keeps the base VLA  
 145 *frozen*. Instead of updating weights online, EFN (i) retrieves a task-relevant experience trajectory,  
 146 (ii) predicts a *residual action* that refines the base policy’s output, and (iii) optimizes the residual  
 147 via dense, similarity-shaped reinforcement signals that compare the observed next frame to the next  
 148 frame in the retrieved trajectory. This design combines the benefits of retrieval (conditioning on  
 149 episodic experience at test time) with residual correction (lightweight, additive refinement), yielding  
 150 a practical path to deployment-time improvement without gradient-based finetuning of the underly-  
 151 ing VLA.

152 **2.3 Embodied Reinforcement Learning**  
 153

154 Embodied reinforcement learning studies how agents acquire control policies through trial-and-error  
 155 interaction with the physical or simulated world, facing challenges such as sparse rewards, sample  
 156 efficiency, and robustness under real-world noise. Classic advances improved learning from sparse  
 157 signals via goal relabeling (Andrychowicz et al., 2017), enabled large-scale real-robot training for  
 158 vision-based manipulation (Bodnar et al., 2020), and accelerated fine-tuning by leveraging offline  
 159 data before online improvement (Nair et al., 2020). Subsequent work emphasized data efficiency  
 160 from pixels through strong regularization and augmentation (Yarats et al., 2021), while model-based  
 161 methods demonstrated broad generality by learning world models that support imagination-based  
 162 policy updates across diverse domains (Hafner et al., 2025). Benchmarks for compositional general-  
 163 ization and knowledge transfer (e.g., LIBERO) have provided standardized axes to evaluate continual

162 improvement and robustness in embodied settings (Liu et al., 2023; Yang et al., 2025; Zhang et al.,  
 163 2024; Garcia et al., 2025).

164 **Our scope.** In contrast to training ever-larger *foundation* VLA policies, our focus is a post-  
 165 deployment mechanism that augments a frozen base policy with *experience-driven* corrections. Con-  
 166 cretely, we optimize an Experience Feedback Network (EFN) that retrieves trajectories from an  
 167 experience bank and outputs a residual action to refine the base control. EFN is trained with re-  
 168 enforcement learning signals shaped by observation similarity, and in this work we instantiate the  
 169 learner with Soft Actor–Critic (SAC) (Haarnoja et al., 2018)—thus *learning an experience-feedback*  
 170 *module* rather than relearning a foundation VLA model.

### 172 3 Preliminaries

174 **Task setting.** We consider an embodied agent that interacts with an environment given a short  
 175 natural-language instruction  $\ell$  (e.g., “*put the cup on the plate*”). At discrete time  $t \in \{0, 1, \dots\}$ ,  
 176 the agent receives an *observation*  $o_t$  and produces an *action*  $a_t$ . In our setting, the observation is  
 177 a single RGB frame (optionally concatenated with proprioceptive states); we write  $o_t := (I_t, x_t)$ ,  
 178 where  $I_t \in \mathbb{R}^{H \times W \times 3}$  is the image and  $x_t$  is any low-dimensional robot state (e.g., gripper opening).  
 179 The environment then transitions according to  $o_{t+1} \sim \mathcal{T}(\cdot | o_t, a_t)$  and emits a (task-dependent)  
 180 terminal signal when the rollout ends.

181 **VLA backbone.** A Vision–Language–Action (VLA) policy maps observations and language to an  
 182 internal representation and a low-level command. We denote it by:

$$184 (Z_t, V_t) = \Pi_{\text{VLA}}(o_t, \ell), \quad Z_t \in \mathbb{R}^{4 \times d}, \quad V_t \in \mathbb{R}^{T \times d}, \quad (1)$$

185 where  $V_t$  are visual tokens (spatial features) and  $Z_t$  are latent action tokens (a short sequence that  
 186 summarizes the intended control for the next step). A fixed decoder  $D_\psi$  converts these latents to a  
 187 continuous control:

$$188 u_t^{\text{base}} = D_\psi(Z_t, V_t). \quad (2)$$

189 Intuitively, equation 1 extracts “what the scene looks like” (via  $V_t$ ) and a proposal for “what to do  
 190 next” (via  $Z_t$ ); equation 2 turns that proposal into motor commands.

192 **Experiences and memory.** We define a single *experience* (also called a trajectory) is the sequence

$$193 E = \{(o_0, a_0), (o_1, a_1), \dots, (o_L, \text{end})\}.$$

194 We maintain an *experience memory*  $\langle E \rangle = \{E^{(1)}, E^{(2)}, \dots\}$  that stores step-level records extracted  
 195 from prior rollouts (e.g., images, visual tokens, latent actions). Given the current tokens  $(V_t, Z_t)$   
 196 and instruction  $\ell$ , a simple retriever selects a step from memory that is most relevant to the current  
 197 situation:

$$198 j^* = \text{retrieve}(V_t, \ell; \langle E \rangle), \quad (V_t^E, Z_t^E, V_{t+1}^E) \leftarrow \langle E \rangle[j^*]. \quad (3)$$

199 Here  $V_t^E$  is the stored visual token matrix of the matched memory step, and  $V_{t+1}^E$  is its immediate  
 200 successor; these provide a concrete *execution prototype* for the current step.

### 202 4 Methodology

#### 204 4.1 Overview of EFN

206 Our EFN framework is shown in Figures 2 for train stage and 3 for test stage. In the following sec-  
 207 tions, we structure the method in four parts for clarity: (1) **Experience Bank and Record Schema**,  
 208 explaining how trajectories are recorded at the step level (images, visual tokens, latent actions),  
 209 pooled into compact keys, and stored for fast constant-time access; (2) **Language-Conditioned**  
 210 **Similarity and Retrieval**, which describes how we compute instruction-aware semantic simi-  
 211 larity to select the most relevant experience step and its successor; (3) **Residual Policy Learning with**  
 212 **SAC**, manifesting how EFN’s actor predicts residual latent actions and is trained with Soft Actor–  
 213 Critic under a dense, token-level similarity reward; and (4) **Deployment-Time Recall and Online**  
 214 **Experience Growth**, which elaborates the inference stage of EFN that runs deterministically, re-  
 215 trievals guidance per step, and appends the most successful (or most promising) new rollouts back  
 into the bank to enable continual improvement without updating base policy weights.

216 4.2 Experience Bank Design  
217

218 **Storage schema.** We organize experiences by full *rollouts*  $\tau = (s_1, a_1, \dots, s_T, a_T)$  and insert  
219 into the bank every non-blank step  $(s_t, a_t)$  encountered during data collection or deployment. Im-  
220 portantly, we do *not* pre-filter by success or failure; the rationale for keeping both kinds of outcomes  
221 (and how we leverage them) is discussed in the appendix. For each rollout  $\tau$  we also store a fixed  
222 *instruction embedding*  $\ell_\tau$  obtained by encoding the task description with the VLA’s language model  
223 at the beginning of the episode. At the step level, we record three items: (i) the VLA vision-encoder  
224 features  $\mathbf{F}_t \in \mathbb{R}^{L \times C}$  for frame  $s_t$  (e.g., token features), (ii) a compact *key* vector  $\mathbf{k}_t \in \mathbb{R}^{d_k}$  derived  
225 from  $\mathbf{F}_t$  for retrieval, and (iii) the base policy’s raw action  $\mathbf{a}_t^{(0)}$  executed at that step. The bank  
226 therefore stores tuples  $(\ell_\tau, \mathbf{F}_t, \mathbf{k}_t, \mathbf{a}_t^{(0)})$  for all valid  $t$  across all trajectories.  
227

228 **Key construction and probabilistic top- $k$  retrieval.** Our key uses a *mean–max fusion with per-*  
229 *vector  $\ell_2$  normalization*. First,  $\ell_2$ -normalize each token feature in  $\mathbf{F}_t$  across channels. Then compute  
230 mean and max along the token dimension and normalize each result:  
231

$$\tilde{\mathbf{F}}_t(\ell, \cdot) = \frac{\mathbf{F}_t(\ell, \cdot)}{\|\mathbf{F}_t(\ell, \cdot)\|_2 + \varepsilon}, \quad \mathbf{m}_t = \frac{\text{mean}_\ell(\tilde{\mathbf{F}}_t(\ell, \cdot))}{\|\text{mean}_\ell(\tilde{\mathbf{F}}_t(\ell, \cdot))\|_2 + \varepsilon}, \quad \mathbf{x}_t = \frac{\max_\ell(\tilde{\mathbf{F}}_t(\ell, \cdot))}{\|\max_\ell(\tilde{\mathbf{F}}_t(\ell, \cdot))\|_2 + \varepsilon}. \quad (4)$$

232 Then we fuse the two by an equal-weight average followed by a final normalization, yielding the  
233 key (here  $d_k = C$ ):  
234

$$\mathbf{k}_t = \frac{\frac{1}{2} \mathbf{m}_t + \frac{1}{2} \mathbf{x}_t}{\|\frac{1}{2} \mathbf{m}_t + \frac{1}{2} \mathbf{x}_t\|_2 + \varepsilon} \in \mathbb{R}^{d_k}. \quad (5)$$

235 At query time, we form a query vector  $\mathbf{q}_t$  from the current frame via the same fusion, compute cosine  
236 similarities  $s_i = \cos(\mathbf{q}_t, \mathbf{k}_i)$  to all keys, and select the top- $k$  indices  $\mathcal{N}_k(\mathbf{q}_t)$ . We then sample one  
237 key from this shortlist with a similarity-biased distribution:  
238

$$p(i \mid \mathbf{q}_t) = \frac{\exp(s_i/\tau)}{\sum_{j \in \mathcal{N}_k(\mathbf{q}_t)} \exp(s_j/\tau)}, \quad i \in \mathcal{N}_k(\mathbf{q}_t), \quad (6)$$

239 where  $\tau > 0$  is a temperature. This “retrieve-then-sample” preserves exploration among near-  
240 matches while favoring the most semantically similar experiences.  
241

242 4.3 Learning EFN with Residual Policy Optimization  
243

244 **Problem setup.** EFN learns to *nudge* the base policy by recalling a relevant past experience and  
245 adjusting the current action so that the next observation resembles “what happened next” in experi-  
246 ence. At step  $t$ , the inputs are: current visual features  $\mathbf{F}_t$  and the base policy’s action  $\mathbf{a}_t^{(0)}$ , together  
247 with a retrieved experience step  $(\hat{\mathbf{F}}, \hat{\mathbf{a}}, \hat{\mathbf{F}}^+)$  and its rollout-level instruction embedding  $\ell$  (retrieval is  
248 defined in the previous subsection). EFN’s actor outputs a residual  $\Delta\mathbf{a}_t$ ; the executed control is  
249

$$\mathbf{a}_t = \mathbf{a}_t^{(0)} + \Delta\mathbf{a}_t. \quad (7)$$

250 Intuitively,  $\mathbf{a}_t^{(0)}$  preserves the base policy’s competence, and  $\Delta\mathbf{a}_t$  is experience-informed correction.  
251

252 **Semantic Match Reward.** To quantify the notion of “match the experience’s next outcome,” we  
253 compare the realized next observation  $s_{t+1}$  with the experience’s successor frame  $\hat{s}^+$  at the *semantic*  
254 level. Let  $\mathbf{u}(\cdot)$  be the mean–max fusion described earlier, applied to vision features to produce a unit  
255 vector. After executing  $\mathbf{a}_t$ , the environment yields  $s_{t+1}$  with vision features  $\mathbf{F}_{t+1}$ . We define a dense  
256 similarity reward  
257

$$r_t^{\text{sem}} = \cos(\mathbf{u}(\mathbf{F}_{t+1}), \mathbf{u}(\hat{\mathbf{F}}^+)). \quad (8)$$

258 In practice we also regularize the residual magnitude to avoid destabilizing the base behavior:  
259

$$r_t = \lambda_{\text{sem}} r_t^{\text{sem}} - \lambda_{\text{res}} \|\Delta\mathbf{a}_t\|_2^2, \quad (9)$$

260 with  $\lambda_{\text{sem}}, \lambda_{\text{res}} > 0$ . This reward directly encodes our training signal without requiring supervised  
261 residual labels; a discussion on why we avoid direct supervision appears in the appendix.  
262

270 **SAC objective.** We train EFN with Soft Actor–Critic, conditioning both actor and critics on the  
 271 current and experience context. Let

$$272 \quad \mathbf{c}_t = \text{enc}(\mathbf{F}_t, \mathbf{a}_t^{(0)}, \hat{\mathbf{F}}, \hat{\mathbf{a}}, \ell) \quad (10)$$

274 be a learned context representation (the base policy is frozen). The stochastic residual policy is  
 275  $\pi_\phi(\Delta \mathbf{a}_t | \mathbf{c}_t)$ , and the Q-functions  $Q_{\theta_1}, Q_{\theta_2}$  evaluate the corrected action  $\mathbf{a}_t = \mathbf{a}_t^{(0)} + \Delta \mathbf{a}_t$  under  $\mathbf{c}_t$ .  
 276 The critic targets use the soft Bellman backup with target networks  $\bar{\theta}_i$ :

$$277 \quad y_t = r_t + \gamma \mathbb{E}_{\Delta \mathbf{a}_{t+1} \sim \pi_\phi(\cdot | \mathbf{c}_{t+1})} \left[ \min_{i=1,2} Q_{\bar{\theta}_i}(\mathbf{c}_{t+1}, \mathbf{a}_{t+1}^{(0)} + \Delta \mathbf{a}_{t+1}) - \alpha \log \pi_\phi(\Delta \mathbf{a}_{t+1} | \mathbf{c}_{t+1}) \right]. \quad (11)$$

280 The critic loss is the standard squared error:

$$281 \quad \mathcal{L}_{\text{critic}}(\theta_1, \theta_2) = \sum_{i=1,2} \mathbb{E} \left[ (Q_{\theta_i}(\mathbf{c}_t, \mathbf{a}_t^{(0)} + \Delta \mathbf{a}_t) - y_t)^2 \right]. \quad (12)$$

284 The actor minimizes the entropy-regularized objective

$$285 \quad \mathcal{L}_{\text{actor}}(\phi) = \mathbb{E}_{\Delta \mathbf{a}_t \sim \pi_\phi(\cdot | \mathbf{c}_t)} \left[ \alpha \log \pi_\phi(\Delta \mathbf{a}_t | \mathbf{c}_t) - \min_{i=1,2} Q_{\theta_i}(\mathbf{c}_t, \mathbf{a}_t^{(0)} + \Delta \mathbf{a}_t) \right], \quad (13)$$

287 with temperature  $\alpha$  optionally tuned to maintain a target entropy. During training, gradients do not  
 288 flow through the retrieval targets  $\hat{\mathbf{F}}, \hat{\mathbf{F}}^+$ ; updates are confined to EFN’s actor, critics, and the context  
 289 encoder.

290 **Reward shaping with anti-idling penalty.** To retain absolute credit for matching the retrieved  
 291 next observation while penalizing “similar but no progress” and encouraging shorter rollouts, we  
 292 define semantic similarities ( $\text{sim} \in [0, 1]$ )

$$294 \quad s_t^{\text{next}} = \text{sim}(\mathbf{F}_{t+1}, \hat{\mathbf{F}}^+), \quad s_t^{\text{cur}} = \text{sim}(\mathbf{F}_t, \hat{\mathbf{F}}), \quad s_t^{\text{stay}} = \text{sim}(\mathbf{F}_{t+1}, \mathbf{F}_t). \quad (14)$$

295 We introduce auxiliary terms (with  $[x]_+ = \max(x, 0)$  and tolerance  $\varepsilon > 0$ ):

$$296 \quad a_t = s_t^{\text{next}}, \quad p_t = s_t^{\text{next}} - s_t^{\text{cur}}, \quad m_t = 1 - s_t^{\text{stay}}, \quad n_t = [\varepsilon - p_t]_+. \quad (15)$$

298 The dense reward becomes

$$299 \quad r_t = w_{\text{abs}} a_t + w_{\text{prog}} [p_t]_+ + w_{\text{mot}} m_t - w_{\text{lazy}} (s_t^{\text{next}} n_t s_t^{\text{stay}}) - \lambda_{\text{time}}, \quad (16)$$

300 where  $w_{\text{abs}}, w_{\text{prog}}, w_{\text{mot}}, w_{\text{lazy}} \geq 0$  and  $\lambda_{\text{time}} \geq 0$  are scalars. Equation equation 16 preserves an *absolute similarity bonus* ( $a_t$ ) so that high next-frame alignment is always rewarded; adds a *progress* term ( $[p_t]_+$ ) to further credit genuine improvement toward the retrieved next state; encourages *non-trivial motion* ( $m_t$ ) to avoid degenerate idling; and introduces a targeted *anti-idling penalty* ( $s_t^{\text{next}} n_t s_t^{\text{stay}}$ ) that activates only when the prediction is already similar yet shows negligible improvement and little change between consecutive frames. The per-step cost  $\lambda_{\text{time}}$  favors shorter successful trajectories. Conceptually, EFN thus learns a residual policy that steers  $\mathbf{F}_{t+1}$  toward  $\hat{\mathbf{F}}^+$ , while avoiding “standing still to farm similarity.”

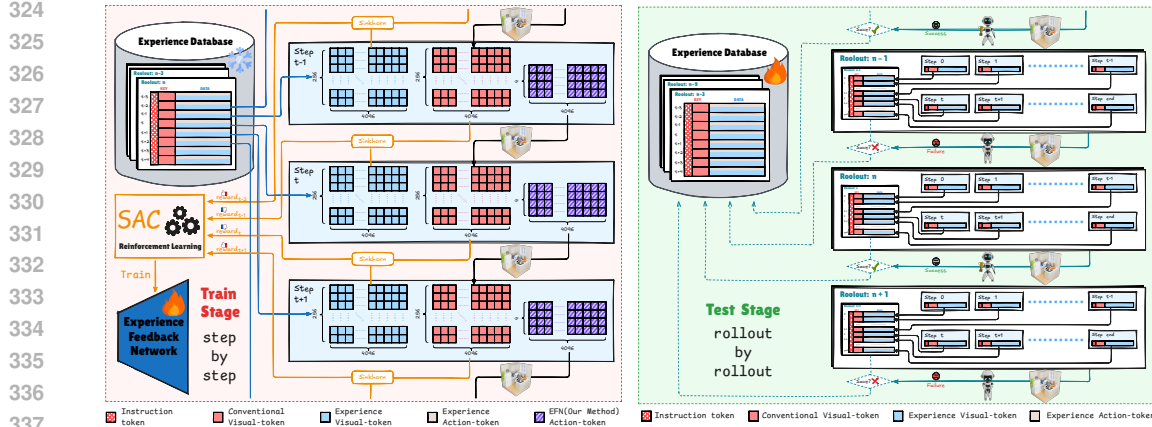
#### 309 4.4 Deployment-Time Retrieval and Online Experience Growth

310 **Goal and key differences.** At deployment, EFN recalls and reuses prior experiences while *not* up-  
 311 dating the base policy’s weights. The inference pipeline mirrors training but differs in three places.  
 312 First, retrieval is *task-filtered*: we restrict matches to rollouts whose instruction embeddings are close  
 313 to the current task. Second, we *prioritize efficient rollouts*: shorter trajectories receive higher selec-  
 314 tion priority because they typically contain fewer redundant actions and lead to faster completion.  
 315 Third, we *grow the bank online*: after a rollout finishes, its non-blank steps are inserted into the bank  
 316 so that future episodes can recall them.

318 **Instruction-filtered candidate set.** Given a task description, we compute an instruction embed-  
 319 ding with the VLA’s language encoder, denoted  $\ell^*$ . We compare  $\ell^*$  to all stored rollout-level em-  
 320 beddings  $\{\ell_{\tau_j}\}$  with cosine similarity and select the top- $n$  rollouts:

$$321 \quad \mathcal{R}_n = \text{Top-}n \left\{ \cos(\ell^*, \ell_{\tau_j}) \right\}_{j=1}^n. \quad (17)$$

323 All step-level entries from these rollouts form the *candidate experience set*  $\mathcal{C}$ , which is the only pool  
 we retrieve from during this episode.



324  
325  
326  
327  
328  
329  
330  
331  
332  
333  
334  
335  
336  
337  
338  
339  
340  
341  
342  
343  
344  
345  
346  
347  
348  
349  
350  
351  
352  
353  
354  
355  
356  
357  
358  
359  
360  
361  
362  
363  
364  
365  
366  
367  
368  
369  
370  
371  
372  
373  
374  
375  
376  
377

Figure 2: EFN trains a residual policy with SAC to nudge the base action so the next frame matches the retrieved memory’s successor.

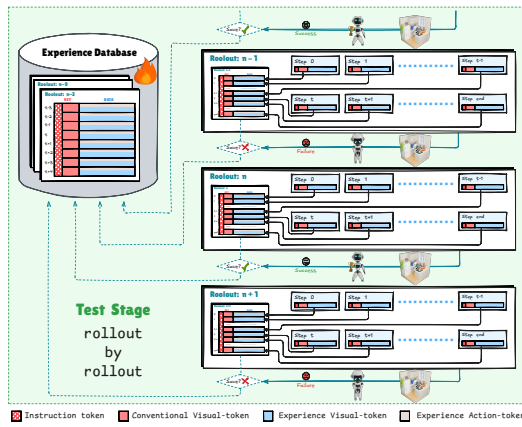


Figure 3: At inference, EFN filters memories by instruction, retrieves efficient candidates, applies the residual correction and grows the bank online.

**Step-wise retrieval with efficiency prior.** At step  $t$ , we form a visual query  $\mathbf{q}_t = \mathbf{u}(\mathbf{F}_t)$  using the mean–max fusion  $\mathbf{u}(\cdot)$  defined previously. Each candidate  $i \in \mathcal{C}$  has a key  $\mathbf{k}_i$ , a successor feature  $\hat{\mathbf{F}}_i^+$ , and belongs to a rollout  $\rho(i)$  with total length  $L_{\rho(i)}$ . We score candidates by combining semantic similarity and an efficiency prior that favors shorter rollouts. Let  $s_i = \cos(\mathbf{q}_t, \mathbf{k}_i)$  and define a normalized length prior  $g(L_{\rho(i)}) \in [0, 1]$  that decreases with  $L_{\rho(i)}$  (e.g.,  $g(L) = \exp[-\beta L / \bar{L}]$  with temperature  $\beta$  and reference length  $\bar{L}$ ). The combined score is

$$\tilde{s}_i = \lambda s_i + (1 - \lambda) g(L_{\rho(i)}), \quad \lambda \in [0, 1]. \quad (18)$$

We take the top- $k$  candidates by  $\tilde{s}_i$  and sample one with softmax:

$$p(i \mid t) = \frac{\exp(\tilde{s}_i / \tau)}{\sum_{j \in \mathcal{N}_k(t)} \exp(\tilde{s}_j / \tau)}, \quad i \in \mathcal{N}_k(t), \quad (19)$$

where  $\tau$  is a temperature and  $\mathcal{N}_k(t)$  denotes the  $k$  highest-scoring items at step  $t$ . This procedure preserves exploration among near-matches while preferring memories that both look similar and come from efficient behaviors.

**Action correction and execution.** Conditioned on the current context and the sampled experience  $(\hat{\mathbf{F}}_i, \hat{\mathbf{a}}_i, \hat{\mathbf{F}}_i^+)$ , EFN predicts a residual  $\Delta \mathbf{a}_t$  and executes  $\mathbf{a}_t = \mathbf{a}_t^{(0)} + \Delta \mathbf{a}_t$  as in training. All critics and the policy remain fixed at inference; if desired, we use a deterministic mean action or a low-temperature sample to reduce variance. The semantic objective from training carries over conceptually: the correction is chosen to steer the next observation toward the stored successor  $\hat{\mathbf{F}}_i^+$ .

**Online experience growth.** After the episode ends, we insert the new rollout into the bank: we store the episode-level instruction embedding  $\ell^*$  with all non-blank step tuples  $(\mathbf{F}_t, \mathbf{k}_t, \mathbf{a}_t^{(0)})$  computed with the same mean–max keying. Consistent with our storage policy, we do not filter by success or failure; reasons and ablations are provided in the appendix. In practice, when operating under a experience budget, one can apply standard retention strategies (e.g., reservoir-style sampling or recency-aware replacement) without changing the retrieval or learning rules described above.

## 5 Experiments

**Experimental Setup** We evaluate EFN in the LIBERO simulator on the `libero_goal` benchmark (Liu et al., 2023). The visuomotor backbone is a pretrained OpenVLA policy executed in bfloat16 with Flash Attention (Dao, 2023). Visual inputs follow the Prismatic pretraining pipeline (center crop; resize to 256). Each episode starts with a 10-step settling period without control. UniVLA provides a sequence of 256 visual tokens and 4 latent action tokens per step over a window of length 12. EFN receives the current tokens and those retrieved from the experience bank; the actor



Figure 4: Visualization of EFN’s residual action: corrections become smaller and more targeted as the bank grows. Within each patch: Left: Original Observation; Middle: Experience Observation; Right: Corrected action vs original action.



Figure 5: AgiBot-G1 platform used in our real-world experiments.

predicts a residual in latent space that is added to the base latent action and decoded by the *frozen* action head. The detailed training protocol can be found in Appendix B.

**Evaluation protocol.** At test time the policy is deterministic by applying tanh to the actor mean in token space. We report success rate and, conditional on success, the average number of steps (lower is better). For `libero_goal` the horizon cap is  $H=320$ . The evaluation-time experience bank mirrors training and is queried via cosine nearest neighbors over pooled visual embeddings. After each successful rollout, we append the episode (images, token features, pooled keys) to the bank; among successes, shorter episodes are retained with higher priority to efficiency.

Table 1: Deployment Performance on Libero Dataset by OpenVLA and UniVLA

Method	Spatial		Object		Goal		Long		Average	
	Succ. $\uparrow$	Step $\downarrow$								
OpenVLA (Kim et al., 2024)	84.7	119.5	88.4	163.7	79.2	121.5	53.7	275.9	76.5	160.2
+EFN(Volume=100)	86.2	117.0	90.1	161.0	81.4	119.4	64.8	270.6	80.6	160.8
+EFN(Volume=300)	88.5	115.4	91.3	158.8	85.7	117.0	72.1	267.2	84.4	160.0
+EFN(Volume=500)	<b>90.2</b>	111.8	92.0	158.3	88.1	<b>114.5</b>	75.7	264.3	86.5	158.2
+EFN(Volume=1000)	89.9	<b>109.0</b>	<b>92.2</b>	<b>156.1</b>	<b>89.2</b>	115.2	<b>76.5</b>	<b>261.9</b>	<b>87.0</b>	<b>156.7</b>
UniVLA (Bu et al., 2025b)	96.5	112.7	96.8	159.0	95.6	124.9	92.0	264.5	95.2	164.2
+EFN(Volume=100)	97.2	107.6	97.4	154.9	96.4	122.2	92.9	258.1	96.0	159.7
+EFN(Volume=300)	97.7	103.4	97.9	151.4	97.2	120.1	93.7	253.8	96.6	156.2
+EFN(Volume=500)	98.1	<b>101.8</b>	<b>98.2</b>	146.7	97.4	<b>117.6</b>	94.3	244.1	97.0	151.7
+EFN(Volume=1000)	<b>98.2</b>	102.1	<b>98.2</b>	<b>145.8</b>	<b>97.6</b>	117.8	<b>94.6</b>	<b>242.5</b>	<b>97.2</b>	<b>151.3</b>

**Baselines and variants.** We compare OpenVLA and UniVLA backbones with and without EFN, and study the effect of bank capacity ( $\text{Volume} \in \{100, 300, 500, 1000\}$ ). Real-world tests are conducted on the AgiBot-G1 platform with the GO-1 policy (Bu et al., 2025a).

**Results on LIBERO.** Tables (OpenVLA/UniVLA) show that adding EFN consistently improves average success while reducing steps, and larger banks yield further gains. Improvements are most pronounced on the Long split, indicating that recall-guided residuals help truncate redundant behavior. UniVLA starts strong and still benefits from EFN, suggesting complementary value between

Table 2: Real-World Experiment of AgiBot G1 Robot with GO-1 model on three tasks

Benchmark	PutBottle		SortItem		AddGoods	
	Succ. $\uparrow$	Step $\downarrow$	Succ. $\uparrow$	Step $\downarrow$	Succ. $\uparrow$	Step $\downarrow$
GO-1 (Bu et al., 2025a)	46.9	411.0	34.3	443.5	15.6	388.0
+EFN(Volume=50)	56.3	398.2	40.6	427.8	28.1	372.1
+EFN(Volume=100)	65.6	386.8	43.8	419.9	34.4	364.4
+EFN(Volume=300)	<b>68.8</b>	383.5	46.9	416.0	40.6	359.2
+EFN(Volume=500)	<b>68.8</b>	<b>379.4</b>	<b>50.0</b>	<b>414.3</b>	<b>43.8</b>	<b>358.0</b>

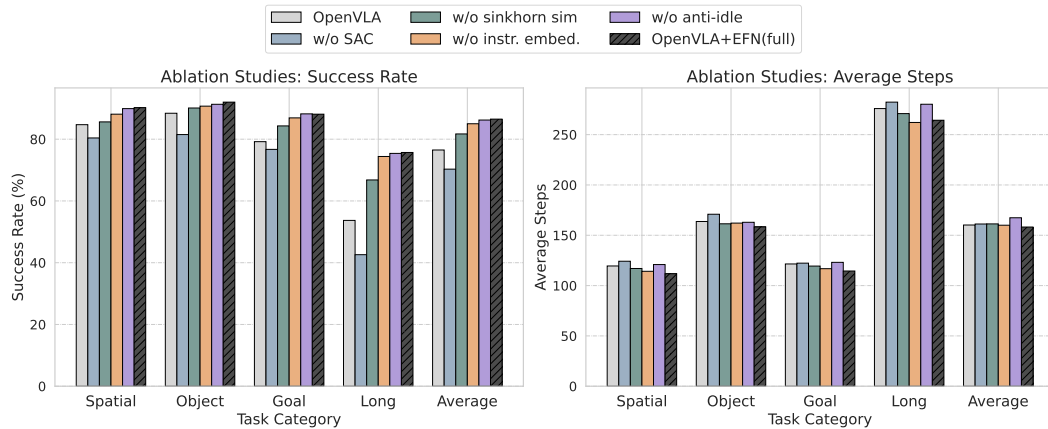


Figure 6: Ablation studies of EFN on Libero Dataset.

a strong backbone and experience-guided correction. Figure 1 visualizes residual actions; qualitatively, EFN produces smaller, more purposeful adjustments as the bank grows. We show the performance of the predicted residual actions in Figure 4.

**Real-world results.** On AgiBot-G1 (Figure 5) across three manipulation tasks, EFN boosts success and shortens trajectories as bank size increases, with diminishing returns beyond a few hundred entries, as shown in Table 2. This aligns with the simulator trend and indicates that EFN’s retrieval-and-correct mechanism transfers to physical systems without changing the frozen backbone. The detailed instructions of these tasks is in Appendix B.

**Ablations.** Our evaluation of four variants validates our design choices. The w/o SAC variant, which replaced SAC with a simpler critic, degraded both success and efficiency, confirming the importance of entropy-regularized optimization. Similarly, the w/o sinkhorn sim variant, using cosine similarity instead of our Sinkhorn OT reward, provided a weaker training signal and lower performance. Removing instruction-based filtering in the w/o instruction embed variant led to retrieval mismatches and consistently underperformed, while dropping the penalty in the w/o anti-idle model increased dithering and average steps. Our conclusion is that these ablations prove each component is critical, with the complete EFN achieving the best overall balance of success and efficiency.

## 6 Conclusion

We introduced the Experience Feedback Network (EFN), which augments a frozen vision–language–action policy with a residual controller and episodic memory. By retrieving semantically relevant trajectories and imitating their next transitions through token-level optimal transport, EFN enables deployment-time adaptation without modifying pretrained weights. This transforms occasional successes into reliable performance and reframes post-deployment learning as case-based control: the backbone provides competence, memory provides context, and the residual head provides adaptation. With advances in memory, retrieval, and credit assignment, experience-driven adaptation offers a promising path to bridge offline generalization and reliable on-site execution for embodied agents.

486  
487 References

- 488 Marcin Andrychowicz et al. Hindsight experience replay. In *Advances in Neural Infor-  
489 mation Processing Systems (NeurIPS)*, 2017. URL <https://proceedings.neurips.cc/paper/7090-hindsight-experience-replay.pdf>.
- 490  
491 Andrea Bacciu, Florin Cuconasu, Federico Siciliano, Fabrizio Silvestri, Nicola Tonello, and  
492 Giovanni Trappolini. Rraml: Reinforced retrieval augmented machine learning, 2023. URL  
493 <https://arxiv.org/abs/2307.12798>.
- 494  
495 Marco Bagatella, Mert Albaba, Jonas Hübotter, Georg Martius, and Andreas Krause. Test-time  
496 offline reinforcement learning on goal-related experience. *CoRR*, abs/2507.18809, 2025. doi:  
497 10.48550/ARXIV.2507.18809. URL <https://doi.org/10.48550/arXiv.2507.18809>.
- 498 Ali Behrouz, Peilin Zhong, and Vahab Mirrokni. Titans: Learning to memorize at test time, 2024.  
499 URL <https://arxiv.org/abs/2501.00663>.
- 500  
501 Cristian Bodnar, Adrian Li, Karol Hausman, Peter Pastor, and Mrinal Kalakrishnan. Quantile QT-  
502 Opt for risk-aware vision-based robotic grasping. In *Robotics: Science and Systems (RSS)*, 2020.  
503 URL <https://roboticsproceedings.org/rss16/p075.pdf>.
- 504 Anthony Brohan et al. Rt-1: Robotics transformer for real-world control at scale. In *Robotics:  
505 Science and Systems (RSS)*, 2023. URL <https://roboticsproceedings.org/rss19/p025.pdf>.
- 506  
507 Qingwen Bu, Jisong Cai, Li Chen, Xiuqi Cui, Yan Ding, Siyuan Feng, Shenyuan Gao, Xindong  
508 He, Xuan Hu, Xu Huang, Shu Jiang, Yuxin Jiang, Cheng Jing, Hongyang Li, Jialu Li, Chiming  
509 Liu, Yi Liu, Yuxiang Lu, Jianlan Luo, Ping Luo, Yao Mu, Yuehan Niu, Yixuan Pan, Jiangmiao  
510 Pang, Yu Qiao, Guanghui Ren, Cheng Ruan, Jiaqi Shan, Yongjian Shen, Chengshi Shi, Mingkang  
511 Shi, Modi Shi, Chonghao Sima, Jianheng Song, Huijie Wang, Wenhao Wang, Dafeng Wei, Chen-  
512 gen Xie, Guo Xu, Junchi Yan, Cunbiao Yang, Lei Yang, Shukai Yang, Maoqing Yao, Jia Zeng,  
513 Chi Zhang, Qinglin Zhang, Bin Zhao, Chengyue Zhao, Jiaqi Zhao, and Jianchao Zhu. Agibot  
514 world colosseo: A large-scale manipulation platform for scalable and intelligent embodied  
515 systems, 2025a. URL <https://arxiv.org/abs/2503.06669>.
- 516  
517 Qingwen Bu, Yanting Yang, Jisong Cai, Shenyuan Gao, Guanghui Ren, Maoqing Yao, Ping Luo, and  
518 Hongyang Li. Univla: Learning to act anywhere with task-centric latent actions. *arXiv preprint  
arXiv:2505.06111*, 2025b.
- 519  
520 Chilam Cheang, Sijin Chen, Zhongren Cui, Yingdong Hu, Liqun Huang, Tao Kong, Hang Li, Yifeng  
521 Li, Yuxiao Liu, Xiao Ma, Hao Niu, Wenxuan Ou, Wanli Peng, Zeyu Ren, Haixin Shi, Jiawen Tian,  
522 Hongtao Wu, Xin Xiao, Yuyang Xiao, Jiafeng Xu, and Yichu Yang. Gr-3 technical report, 2025.  
523 URL <https://arxiv.org/abs/2507.15493>.
- 524 Tri Dao. Flashattention-2: Faster attention with better parallelism and work partitioning, 2023. URL  
525 <https://arxiv.org/abs/2307.08691>.
- 526  
527 Roya Firooz, Johnathan Tucker, Stephen Tian, Anirudha Majumdar, Jiankai Sun, Weiyu Liu,  
528 Yuke Zhu, Shuran Song, Ashish Kapoor, Karol Hausman, Brian Ichter, Danny Driess, Jia-  
529 jun Wu, Cewu Lu, and Mac Schwager. Foundation models in robotics: Applications, chal-  
530 lenges, and the future. *Int. J. Rob. Res.*, 44(5):701–739, April 2025. ISSN 0278-3649. doi:  
531 10.1177/02783649241281508. URL <https://doi.org/10.1177/02783649241281508>.
- 532  
533 Ricardo Garcia, Shizhe Chen, and Cordelia Schmid. Towards generalizable vision-language robotic  
534 manipulation: A benchmark and llm-guided 3d policy. In *International Conference on Robotics  
and Automation (ICRA)*, 2025.
- 535 Anirudh Goyal, Abram L. Friesen, Andrea Banino, Theophane Weber, Nan Rosemary Ke,  
536 Adria Puigdomenech Badia, Arthur Guez, Mehdi Mirza, Peter C. Humphreys, Ksenia  
537 Konyushkova, Laurent Sifre, Michal Valko, Simon Osindero, Timothy Lillicrap, Nicolas Heess,  
538 and Charles Blundell. Retrieval-augmented reinforcement learning. In *International Conference  
539 on Machine Learning (ICML)*, volume 162 of *Proceedings of Machine Learning Research*, pp.  
7740–7765, 2022. URL <https://proceedings.mlr.press/v162/goyal22a.html>.

- 540 Huy Ha et al. Octo: An open-source generalist robot policy. In *Robotics: Science and Systems (RSS)*,  
 541 2024. URL <https://roboticsproceedings.org/rss20/p090.pdf>.
- 542
- 543 Tuomas Haarnoja, Aurick Zhou, Pieter Abbeel, and Sergey Levine. Soft actor-critic: Off-policy  
 544 maximum entropy deep reinforcement learning with a stochastic actor. In *International Conference on Machine Learning (ICML)*, volume 80 of *Proceedings of Machine Learning Research*,  
 545 pp. 1861–1870, 2018. URL <https://proceedings.mlr.press/v80/haarnoja18b.html>.
- 546
- 547 Danijar Hafner, Jurgis Pasukonis, Jimmy Ba, and Timothy P. Lillicrap. Mastering diverse control  
 548 tasks through world models. *Nature*, 626(8000), 2025. doi: 10.1038/s41586-025-08744-2. URL  
 549 <https://www.nature.com/articles/s41586-025-08744-2>.
- 550
- 551 Xiaofeng Han, Shunpeng Chen, Zenghuang Fu, Zhe Feng, Lue Fan, Dong An, Changwei Wang,  
 552 Li Guo, Weiliang Meng, Xiaopeng Zhang, Rongtao Xu, and Shibiao Xu. Multimodal fusion and  
 553 vision–language models: A survey for robot vision. *Information Fusion*, 126:103652, 2026. ISSN  
 554 1566-2535. doi: <https://doi.org/10.1016/j.inffus.2025.103652>.
- 555
- 556 T. Johannink et al. Residual reinforcement learning for robot control. In *IEEE International Conference on Robotics and Automation (ICRA)*, 2019. doi: 10.1109/ICRA.2019.8793602.
- 557
- 558 Moo Jin Kim, Karl Pertsch, Siddharth Karamcheti, Ted Xiao, Ashwin Balakrishna, Suraj Nair, Rafael  
 559 Rafailov, Ethan Paul Foster, Pannag R. Sanketi, Quan Vuong, Thomas Kollar, Benjamin Burch-  
 560 fiel, Russ Tedrake, Dorsa Sadigh, Sergey Levine, Percy Liang, and Chelsea Finn. Openvla: An  
 561 open-source vision-language-action model. In Pukit Agrawal, Oliver Kroemer, and Wolfram  
 562 Burgard (eds.), *Conference on Robot Learning, 6-9 November 2024, Munich, Germany*, volume 270 of *Proceedings of Machine Learning Research*, pp. 2679–2713. PMLR, 2024. URL  
 563 <https://proceedings.mlr.press/v270/kim25c.html>.
- 564
- 565 Diederik P. Kingma and Jimmy Ba. Adam: A method for stochastic optimization, 2017. URL  
 566 <https://arxiv.org/abs/1412.6980>.
- 567
- 568 Bo Liu, Yifeng Zhu, Chongkai Gao, Yihao Feng, Qiang Liu, Yuke Zhu, and Peter  
 569 Stone. Libero: Benchmarking knowledge transfer for lifelong robot learning. In  
 570 *Advances in Neural Information Processing Systems (NeurIPS) — Datasets and Bench-  
 marks*, 2023. URL [https://proceedings.neurips.cc/paper\\_files/paper/2023/file/8c3c666820ea055a77726d66fc7d447f-Paper-Datasets\\_and\\_Benchmarks.pdf](https://proceedings.neurips.cc/paper_files/paper/2023/file/8c3c666820ea055a77726d66fc7d447f-Paper-Datasets_and_Benchmarks.pdf).
- 571
- 572 Hao Liu et al. Embodied intelligence: A synergy of morphology, action, and learning. *ACM Computing Surveys*, 2025a. doi: 10.1145/3717059. URL <https://dl.acm.org/doi/10.1145/3717059>.
- 573
- 574
- 575 Huihan Liu, Soroush Nasiriany, Lance Zhang, Zhiyao Bao, and Yuke Zhu. Robot learning on the  
 576 job: Human-in-the-loop autonomy and learning during deployment. *The International Journal  
 577 of Robotics Research*, 2024a. doi: 10.1177/02783649241273901. URL <https://journals.sagepub.com/doi/full/10.1177/02783649241273901>.
- 578
- 579 Jiaming Liu et al. Robomamba: Efficient vision-language-action model for robotic reason-  
 580 ing and manipulation. In *Advances in Neural Information Processing Systems (NeurIPS)*,  
 581 2024b. URL [https://proceedings.neurips.cc/paper\\_files/paper/2024/file/46a126492ea6fb87410e55a58df2e189-Paper-Conference.pdf](https://proceedings.neurips.cc/paper_files/paper/2024/file/46a126492ea6fb87410e55a58df2e189-Paper-Conference.pdf).
- 582
- 583 Zhenxian Liu, Peixi Peng, and Yonghong Tian. Visual reinforcement learning with residual action.  
 584 In Toby Walsh, Julie Shah, and Zico Kolter (eds.), *AAAI-25, Sponsored by the Association for the  
 585 Advancement of Artificial Intelligence, February 25 - March 4, 2025, Philadelphia, PA, USA*, pp.  
 586 19050–19058. AAAI Press, 2025b. doi: 10.1609/AAAI.V39I18.34097. URL <https://doi.org/10.1609/aaai.v39i18.34097>.
- 587
- 588 Ashvin Nair, Murtaza Dalal, Abhishek Gupta, and Sergey Levine. AWAC: Accelerating online rein-  
 589 force learning with offline datasets. In *Advances in Neural Information Processing Systems  
 590 (NeurIPS)*, 2020. URL <https://www.robot-learning.ml/2020/files/D8.pdf>.
- 591
- 592 Junhyuk Oh, Yijie Guo, Satinder Singh, and Honglak Lee. Self-imitation learning. In *International  
 593 Conference on Machine Learning (ICML)*, volume 80 of *Proceedings of Machine Learning Research*,  
 594 pp. 3878–3887, 2018. URL <https://proceedings.mlr.press/v80/oh18b.html>.

- 594 Wilbert Pumacay, Ishika Singh, Jiafei Duan, Ranjay Krishna, Jesse Thomason, and Dieter Fox. The  
 595 colosseum: A benchmark for evaluating generalization for robotic manipulation. *arXiv preprint*  
 596 *arXiv:2402.08191*, 2024. URL <https://arxiv.org/abs/2402.08191>.
- 597 Rui Shao, Wei Li, Lingsen Zhang, Renshan Zhang, Zhiyang Liu, Ran Chen, and Liqiang Nie. Large  
 598 vlm-based vision-language-action models for robotic manipulation: A survey, 2025. URL <https://arxiv.org/abs/2508.13073>.
- 600 Mustafa Shukor, Dana Aubakirova, Francesco Capuano, Pepijn Kooijmans, Steven Palma, Adil  
 601 Zouitine, Michel Aractingi, Caroline Pascal, Martino Russi, Andres Marafioti, Simon Alibert,  
 602 Matthieu Cord, Thomas Wolf, and Remi Cadene. Smolvla: A vision-language-action model for  
 603 affordable and efficient robotics, 2025. URL <https://arxiv.org/abs/2506.01844>.
- 604 Denis Tarasov, Alexander Nikulin, Ilya Zisman, Albina Klepach, Andrei Polubarov, Nikita  
 605 Lyubaykin, Alexander Derevyagin, Igor Kiselev, and Vladislav Kurenkov. Yes, q-learning helps  
 606 offline in-context rl, 2025. URL <https://arxiv.org/abs/2502.17666>.
- 607 Rishit Toteja, Arindam Sarkar, and Prakash Mandayam Comar. In-context reinforcement learning  
 608 with retrieval-augmented generation for text-to-SQL. In Owen Rambow, Leo Wanner, Marianna  
 609 Apidianaki, Hend Al-Khalifa, Barbara Di Eugenio, and Steven Schockaert (eds.), *Proceedings of*  
 610 *the 31st International Conference on Computational Linguistics*, pp. 10390–10397, Abu Dhabi,  
 611 UAE, January 2025. Association for Computational Linguistics. URL <https://aclanthology.org/2025.coling-main.692/>.
- 612 Jiayin Wang, Zhiqiang Guo, Weizhi Ma, and Min Zhang. How far can llms improve from  
 613 experience? measuring test-time learning ability in llms with human comparison. *CoRR*,  
 614 abs/2506.14448, 2025. doi: 10.48550/ARXIV.2506.14448. URL <https://doi.org/10.48550/arXiv.2506.14448>.
- 615 Yue Wang et al. Embodied artificial intelligence: A comprehensive review. *Artificial Intelligence  
 616 Research*, 2024. URL <https://www.scipen.com/article/10.37188/CAAI.2024.018>.
- 617 Rui Yang, Hanyang Chen, Junyu Zhang, Mark Zhao, Cheng Qian, Kangrui Wang, Qineng Wang,  
 618 Teja Venkat Koripella, Marziyeh Movahedi, Manling Li, Heng Ji, Huan Zhang, and Tong Zhang.  
 619 Embodiedbench: Comprehensive benchmarking multi-modal large language models for vision-  
 620 driven embodied agents. In *Forty-second International Conference on Machine Learning*, 2025.  
 621 URL <https://openreview.net/forum?id=DgGF2LEBPS>.
- 622 Denis Yarats, Rob Fergus, Alessandro Lazaric, and Lerrel Pinto. Mastering visual continuous  
 623 control: Improved data-augmented reinforcement learning. In *International Conference on Learning  
 624 Representations (ICLR)*, 2021. URL <https://openreview.net/forum?id=GY6-6sTvGaf>.
- 625 Andy Zhai, Brae Liu, Bruno Fang, Chalse Cai, Ellie Ma, Ethan Yin, Hao Wang, Hugo Zhou, James  
 626 Wang, Lights Shi, Lucy Liang, Make Wang, Qian Wang, Roy Gan, Ryan Yu, Shalfun Li, Starrick  
 627 Liu, Sylas Chen, Vincent Chen, and Zach Xu. Igniting vlms toward the embodied space, 2025.  
 628 URL <https://arxiv.org/abs/2509.11766>.
- 629 Dapeng Zhang, Jin Sun, Chenghui Hu, Xiaoyan Wu, Zhenlong Yuan, Rui Zhou, Fei Shen, and Qing-  
 630 guo Zhou. Pure vision language action (vla) models: A comprehensive survey, 2025. URL  
 631 <https://arxiv.org/abs/2509.19012>.
- 632 Shiduo Zhang, Zhe Xu, Peiju Liu, Xiaopeng Yu, Yuan Li, Qinghui Gao, Zhaoye Fei, Zhangyue  
 633 Yin, Zuxuan Wu, Yu-Gang Jiang, and Xipeng Qiu. Vlabench: A large-scale benchmark for  
 634 language-conditioned robotics manipulation with long-horizon reasoning tasks, 2024. URL  
 635 <https://arxiv.org/abs/2412.18194>.
- 636 Ethan Z. Zitkovich et al. Rt-2: Vision-language-action models transfer web knowledge to robotic  
 637 control. In *Conference on Robot Learning (CoRL)*, volume 229 of *Proceedings of Machine  
 638 Learning Research*, pp. 1742–1768, 2023. URL <https://proceedings.mlr.press/v229/zitkovich23a.html>.

# Appendix

## A Discussion

### A.1 Limitations

The proposed framework inherits a set of practical and conceptual limitations. The first limitation concerns memory growth and curation. The experience memory expands as deployment proceeds, which increases retrieval latency and the risk of recalling suboptimal or redundant prototypes. The current policy mitigates this by prioritizing successful and shorter episodes within task buckets; however, this heuristic does not guarantee global optimality and may discard rare but informative failures. A second limitation is retrieval ambiguity. When the instruction is broad or when multiple experiences are semantically close, the nearest-neighbour criterion can select a trajectory whose next state is misaligned with the current phase, which introduces non-stationary targets for the critic and may slow policy improvement. The third limitation is the cold-start condition. If the bank contains no success and only weak partial progress, the agent may imitate unhelpful behaviours, which delays the discovery of the first success that bootstraps reliable performance. The fourth limitation lies in the reliance on visual token alignment. The imitation reward assumes that the next observation from the current attempt can be meaningfully matched to the next observation of the retrieved experience; strong viewpoint or lighting shifts can degrade the signal, and while entropic optimal transport provides robustness, it adds computational overhead. The fifth limitation is stability of residual control. Large residuals in latent space may push the decoder into regimes insufficiently covered by pretraining; the tanh squashing and action clipping provide safeguards, yet the residual head may still overshoot when the retrieved prototype poorly represents the present scene. Finally, the method trades statistical updates of the frozen backbone for case-based recall; this avoids catastrophic forgetting but also constrains asymptotic optimality when truly new skills beyond the backbone’s representational capacity are required.

### A.2 Future directions

Several extensions can address the above limitations. Memory can be made adaptive through online clustering with diversity-aware reservoir sampling that preserves both canonical successes and atypical but useful corner cases. Retrieval can be learned end-to-end with a contrastive objective that aligns the query embedding of the current state with embeddings of experiences that yielded high downstream imitation rewards, while repelling confounding near-misses; a learned temperature can emphasize discriminative dimensions for disambiguation. Phase awareness can be strengthened by aligning short sub-segments instead of single steps, using dynamic time warping in the token space to stabilize the reference index. The residual policy can incorporate uncertainty estimates to attenuate residual magnitudes when retrieval confidence is low, shifting execution weight back to the frozen backbone until a confident prototype is found. Long-horizon tasks can benefit from compositional recall that stitches segments from multiple experiences into a temporally consistent pseudo-plan, with consistency enforced by overlap constraints in token space. The Sinkhorn computation can be accelerated by low-rank kernel approximations and token pruning schedules that keep only salient patches identified by language-conditioned attention. Finally, safety and interpretability can be improved by attributing which retrieved tokens and which residual channels most affected the decoded action, enabling human oversight and selective memory editing.

Table 3: Ablation Studies on Libero Dataset

Method	Spatial		Object		Goal		Long		Average	
	Succ.	Step								
OpenVLA	84.7	119.5	88.4	163.7	79.2	121.5	53.7	275.9	76.5	160.2
w/o SAC	80.4	124.2	81.5	170.9	76.7	122.3	42.6	282.3	70.3	161.2
w/o sinkhorn sim	85.6	117.0	90.1	161.4	84.3	119.4	66.8	270.9	81.7	161.3
w/o instruction embed	88.1	114.2	90.7	162.1	86.9	116.8	74.4	<b>262.1</b>	85.0	160.0
w/o anti-idle	89.9	120.9	91.3	162.9	<b>88.2</b>	123.1	75.4	280.2	86.2	167.4
OpenVLA+EFN(full)	<b>90.2</b>	<b>111.8</b>	<b>92.0</b>	<b>158.3</b>	88.1	<b>114.5</b>	<b>75.7</b>	264.3	<b>86.5</b>	<b>158.2</b>

702 **B Training Protocol**  
 703

704 We train EFN with goal-conditioned Soft Actor–Critic (SAC). The actor is a lightweight transformer  
 705 with cross-attention over current and retrieved tokens (embed dim 1024, 16 heads, FFN size 4096, 2  
 706 layers with residual connections and LayerNorm). The twin critics pool visual tokens with a multi-  
 707 latent attention block and project current latent, retrieved latent, and residual into a shared 512-d  
 708 space before an MLP head (hidden 1024). The replay buffer stores  $(x_t, \tilde{x}_t, y_t, r_t, d_t)$ , where  $x_t$  are  
 709 current tokens,  $\tilde{x}_t$  retrieved tokens,  $y_t$  the residual target (reparameterized via the actor),  $r_t$  the token-  
 710 level optimal-transport reward, and  $d_t$  the termination flag. We use batch size 32, discount  $\gamma=0.98$ ,  
 711 target update  $\tau=0.005$ , and Adam (Kingma & Ba, 2017) with learning rate  $3 \times 10^{-4}$  for actor, critics,  
 712 and temperature; the target entropy is set to a quarter of the residual degrees of freedom. To reduce  
 713 target drift, the retrieved reference within an episode can be frozen to a stepwise-advanced index.  
 714 The Sinkhorn-based similarity uses entropic regularization  $\varepsilon=0.05$  and 50 iterations; the reward is  
 715 linearly mapped

$$R_t = \alpha(\text{sinkhorn}(X_t, \tilde{X}_t) - \beta), \quad (20)$$

716 with default  $\alpha=1, \beta=0$ .  
 717

718 **Specific Task Description** The prompts of the three tasks are as follow: PutBottle: Grasp the  
 719 drink bottle from the shelf using your right arm. Place the bottle next to similar items on the shelf and  
 720 release the right arm gripper. SortItem: Pick up the drink bottle from the small tabletop with right  
 721 arm. Place the drink bottles on the shelf with your right arm. AddGoods: Grasp the water bottle  
 722 with your right arm. Place the water bottle in the box with your right arm.  
 723

724 **C Why We Do Not Use Supervised Learning**  
 725

726 **Non-differentiable environment dynamics.** EFN predicts a residual  $\mathbf{r}_\theta$  that is *added* to the base  
 727 action  $\mathbf{a}_t$  and then *executed* in the environment:  
 728

$$\mathbf{a}_t^{\text{efn}} = \mathbf{a}_t + \mathbf{r}_\theta \left( \underbrace{\mathbf{o}_t, \mathbf{a}_t}_{\text{current}}, \underbrace{\tilde{\mathbf{o}}_t, \tilde{\mathbf{a}}_t}_{\text{retrieved}} \right), \quad \mathbf{o}_{t+1} \sim \mathcal{T}(\mathbf{o}_t, \mathbf{a}_t^{\text{efn}}), \quad (21)$$

732 where  $\mathcal{T}$  is the (stochastic) transition kernel of the *real* environment. Our learning signal measures  
 733 how close the realized next observation is to the memory’s next observation, e.g.,

$$\ell(\mathbf{o}_{t+1}, \tilde{\mathbf{o}}_{t+1}) = 1 - \text{sim}(f(\mathbf{o}_{t+1}), f(\tilde{\mathbf{o}}_{t+1})), \quad (22)$$

736 with  $f(\cdot)$  a frozen visual encoder and  $\text{sim}$  a cosine (or token-wise) similarity. A naive supervised  
 737 objective would minimize  $\ell$  w.r.t.  $\theta$  by backpropagating through the execution in equation 21. How-  
 738 ever, this requires the Jacobian  $\frac{\partial \mathbf{o}_{t+1}}{\partial \mathbf{a}_t^{\text{efn}}}$  and, via the chain rule,  
 739

$$\frac{\partial \ell}{\partial \theta} = \frac{\partial \ell}{\partial \mathbf{o}_{t+1}} \cdot \underbrace{\frac{\partial \mathbf{o}_{t+1}}{\partial \mathbf{a}_t^{\text{efn}}}}_{\text{env. dynamics}} \cdot \frac{\partial \mathbf{a}_t^{\text{efn}}}{\partial \theta}. \quad (23)$$

744 In physical systems (and most simulators we rely on at train time),  $\mathcal{T}$  is a black box with contact,  
 745 saturation, and sensor quantization; the derivative  $\frac{\partial \mathbf{o}_{t+1}}{\partial \mathbf{a}_t^{\text{efn}}}$  is undefined or prohibitively noisy.  
 746 Consequently, gradients in equation 23 are unavailable, and supervised backpropagation to  $\theta$  be-  
 747 comes infeasible.

748 **Discrete retrieval and credit assignment.** EFN conditions on a *retrieved* memory step chosen by  
 749 a top- $k$  / argmax rule  
 750

$$(\tilde{\mathbf{o}}_t, \tilde{\mathbf{a}}_t, \tilde{\mathbf{o}}_{t+1}) = \arg \underset{i}{\text{top-}k \text{ score}}(g(\mathbf{o}_t, \text{text}), g(\mathbf{o}^i, \text{text}^i)),$$

753 which is a discrete operation. Even if  $\mathcal{T}$  were differentiable, the retrieval introduces another non-  
 754 differentiable node, further breaking end-to-end supervised learning. Moreover, supervised targets  
 755 for residuals are *not identifiable*: many different residuals can lead to next observations that are  
 semantically close to  $\tilde{\mathbf{o}}_{t+1}$ , so a single “ground-truth residual” label does not exist.

756 **RL objective circumvents the need for env gradients.** We therefore pose learning as entropy-  
 757 regularized RL over continuous actions, optimizing the expected semantic reward  
 758

$$759 \quad r(\mathbf{o}_t, \mathbf{a}_t^{\text{efn}}) = \text{sim}(f(\mathbf{o}_{t+1}), f(\tilde{\mathbf{o}}_{t+1})), \quad J(\theta) = \mathbb{E} \left[ \sum_t \gamma^t r(\mathbf{o}_t, \mathbf{a}_t^{\text{efn}}) \right], \quad (24)$$

760 and training EFN’s residual policy with Soft Actor–Critic (SAC). Using the reparameterization  $\mathbf{a}_t^{\text{efn}} =$   
 761  $\mu_\theta(\mathbf{s}_t) + \sigma_\theta(\mathbf{s}_t) \odot \epsilon$ , we maximize

$$762 \quad \mathbb{E} \left[ Q_\phi(\mathbf{s}_t, \mathbf{a}_t^{\text{efn}}) - \alpha \log \pi_\theta(\mathbf{a}_t^{\text{efn}} | \mathbf{s}_t) \right], \quad \mathbf{s}_t = (\mathbf{o}_t, \mathbf{a}_t, \tilde{\mathbf{o}}_t, \tilde{\mathbf{a}}_t), \quad (25)$$

763 where  $Q_\phi$  is learned off-policy. Critically, policy gradients estimate  $\nabla_\theta J$  from *sampled rollouts* and  
 764 do not require differentiating through  $\mathcal{T}$  or the discrete retrieval. This avoids the gradient discontinuities of supervised training, provides proper temporal credit assignment, and remains stable under  
 765 real-world non-smooth dynamics.

766 **Practical remarks.** (1) Differentiable simulators could, in principle, provide  $\partial \mathbf{o}_{t+1} / \partial \mathbf{a}$ , but model  
 767 mismatch and contact non-smoothness introduce severe bias; learned world-models add compounding  
 768 error. (2) Labeling residuals from logged data is unreliable because the base state  $\mathbf{o}_t$  rarely  
 769 matches the retrieved memory state  $\tilde{\mathbf{o}}_t$  exactly; small state mismatch produces large label noise. (3)  
 770 Off-policy SAC lets us reuse experience efficiently while shaping dense rewards from equation 22,  
 771 achieving sample-efficient training without supervised targets.

## 772 D Language conditioned image semantic similarity

773 This appendix details a training free procedure for computing the semantic proximity between two  
 774 visual observations under a short natural language instruction. The method is designed to be plug  
 775 and play inside an experience retrieval loop and to be both storage efficient and computationally light  
 776 at scale.

### 777 D.1 Problem statement and notation

778 Let an observation  $o$  consist of an RGB image  $I$  and optional side signals. In the vision encoder, a  
 779 single frame produces a matrix of token features

$$780 \quad V \in \mathbb{R}^{T \times H}, \quad T = 256, \quad H = 4096, \quad (26)$$

781 where rows index spatial tokens and columns index feature channels. Given two observations  $o_1, o_2$   
 782 and a short instruction  $L$  such as *put the cup on the plate*, the objective is a scalar similarity  $S(o_1, o_2 |$   
 783  $L) \in [0, 1]$  that is high only when both observations depict the same instruction specific semantics.  
 784 The procedure follows a coarse to fine decomposition

$$785 \quad S(o_1, o_2 | L) = S_{\text{embed}}(o_1, o_2) \oplus S_{\text{image}}(o_1, o_2 | L) \oplus S_{\text{act}}(o_1, o_2), \quad (27)$$

786 with a fusion operator specified later.

### 787 D.2 Token pooling on the spatial axis

788 Each column of  $V$  encodes a channel in the learned semantic basis. Each row encodes a spatial  
 789 token that captures local appearance and relations. A global summary that preserves the semantic  
 790 basis should remove spatial redundancy while keeping the channel space intact. Pooling across the  
 791 token axis achieves that outcome. Pooling across channels instead would collapse the learned basis  
 792 and produce a length  $T$  vector of patch magnitudes with poor semantic fidelity.

793 The spatial pooling is defined by per token normalization followed by mean and max aggregation

$$794 \quad \tilde{V}_{i:} = \frac{V_{i:}}{\|V_{i:}\|_2 + \epsilon}, \quad m = \frac{1}{T} \sum_{i=1}^T \tilde{V}_{i:}, \quad x = \max_{1 \leq i \leq T} \tilde{V}_{i:}, \quad (28)$$

$$795 \quad u_0 = \frac{\frac{1}{2} \frac{m}{\|m\|_2 + \epsilon} + \frac{1}{2} \frac{x}{\|x\|_2 + \epsilon}}{\|\frac{1}{2} \frac{m}{\|m\|_2 + \epsilon} + \frac{1}{2} \frac{x}{\|x\|_2 + \epsilon}\|_2 + \epsilon} \in \mathbb{R}^H. \quad (29)$$

796 The vector  $u_0$  is a global semantic descriptor in the model feature space.

810  
 811 **Random projection and quantization for storage efficiency** To reduce storage while preserving  
 812 cosine geometry, apply a fixed Johnson Lindenstrauss projection  $P \in \mathbb{R}^{H \times d}$  with  $d \ll H$  drawn  
 813 once with a fixed seed and stored alongside the dataset

814 
$$u = \frac{u_0 P}{\|u_0 P\|_2 + \varepsilon} \in \mathbb{R}^d. \quad (30)$$
  
 815

816 A per vector symmetric quantizer stores  $u$  as  $(q, s)$  with  
 817

818 
$$s = \frac{\max_j |u_j|}{127} + \delta, \quad q_j = \text{round}\left(\frac{u_j}{s}\right) \in \{-127, \dots, 127\}, \quad (31)$$
  
 819

820 and dequantization  $\hat{u} = s q$ . With  $d = 256$  this yields 256 bytes for  $q$  plus 4 bytes for  $s$  per step before  
 821 compression. For two hundred thousand steps the footprint is roughly fifty to sixty megabytes.  
 822

823 **Coarse similarity** The coarse similarity is the cosine between dequantized summaries  
 824

825 
$$S_{\text{embed}}(o_1, o_2) = \frac{1}{2} \left( 1 + \frac{\hat{u}_1^\top \hat{u}_2}{\|\hat{u}_1\|_2 \|\hat{u}_2\|_2} \right). \quad (32)$$
  
 826

827 **D.3 Language aware image reranking**

828 Let  $z_1, z_2 \in \mathbb{R}^{d_z}$  be image features from a contrastive vision language encoder and let  $t \in \mathbb{R}^{d_z}$  be  
 829 the text feature of  $L$ . Define three components. The appearance proximity  
 830

831 
$$S_{\text{clip}} = \frac{1}{2} \left( 1 + \frac{z_1^\top z_2}{\|z_1\|_2 \|z_2\|_2} \right). \quad (33)$$
  
 832

833 The instruction gate that is stringent on both images  
 834

835 
$$S_{\text{text}} = \min \left\{ \frac{1}{2} \left( 1 + \frac{z_1^\top t}{\|z_1\|_2 \|t\|_2} \right), \frac{1}{2} \left( 1 + \frac{z_2^\top t}{\|z_2\|_2 \|t\|_2} \right) \right\}. \quad (34)$$
  
 836

837 The relation consistency that compares geometric and contact attributes extracted under  $L$ . Let  $r_i \in$   
 838  $\mathbb{R}^K$  collect proximity, intersection over union, contact proxy and gripper opening when available.  
 839 Define  
 840

841 
$$S_{\text{rel}} = \exp \left( - \sum_{k=1}^K \frac{(r_{1k} - r_{2k})^2}{2\sigma_k^2} \right). \quad (35)$$
  
 842

843 The reranking score is a convex combination  
 844

845 
$$S_{\text{image}} = \alpha_c S_{\text{clip}} + \alpha_t S_{\text{text}} + \alpha_r S_{\text{rel}}, \quad \alpha_c, \alpha_t, \alpha_r \geq 0, \quad \alpha_c + \alpha_t + \alpha_r = 1. \quad (36)$$
  
 846

847 If relation cues are absent the weights are renormalized over the remaining terms.  
 848

849 **Relation features** Let  $B_g$  and  $B_o$  denote the gripper and target boxes obtained using open vocabulary  
 850 detection with a query set derived from  $L$ . Let  $c(\cdot)$  return the box center and let  $D$  be the image  
 851 diagonal. Define normalized distance  $d = \|c(B_g) - c(B_o)\|_2/D$ , intersection over union iou and a  
 852 soft contact proxy  $c^* = \max\{\text{iou}, 1 - 3d\}$  clipped to  $[0, 1]$ . The vector  $r$  is  $[1 - d, \text{iou}, c^*, \text{open}]$   
 853 with the last entry taken from robot telemetry if available.  
 854

855 **D.4 Optional phase alignment from latent actions**

856 When latent action tokens  $A \in \mathbb{R}^{4 \times H}$  are recorded, a phase similarity can be computed by averaging  
 857 across the four tokens and applying cosine  
 858

859 
$$S_{\text{act}} = \frac{1}{2} \left( 1 + \frac{\bar{a}_1^\top \bar{a}_2}{\|\bar{a}_1\|_2 \|\bar{a}_2\|_2} \right), \quad \bar{a} = \frac{1}{4} \sum_{j=1}^4 A_{j:}. \quad (37)$$
  
 860

864 D.5 Fusion strategies  
865866 The default additive fusion is  
867

868 
$$S = w_e S_{\text{embed}} + w_i S_{\text{image}} + w_a S_{\text{act}}, \quad w_e, w_i, w_a \geq 0, w_e + w_i + w_a = 1. \quad (38)$$

869 In applications where the coarse descriptor must upper bound the final score one can prefer a gated  
870 composition

871 
$$S = (\alpha + (1 - \alpha) S_{\text{image}}) S_{\text{embed}} + \beta S_{\text{act}}, \quad (39)$$

872 with  $\alpha \in [0, 1]$  and a small  $\beta$ . This preserves identity on duplicate frames when  $S_{\text{embed}} \approx 1$  and  
873 allows the reranker to suppress false positives.874 D.6 Complexity and storage  
875876 With per step summary  $(q, s)$  in dimension  $d$ , coarse retrieval requires a single dequantization and a  
877 cosine in  $O(d)$ . Large scale search uses an approximate nearest neighbor index on  $\hat{u}$ . The reranker  
878 is applied only to the top candidates and uses one forward pass of the vision language encoder and  
879 one run of open vocabulary detection when relation cues are enabled.  
880881 For a dataset with  $N$  steps the storage for summaries is about  $N \times (d + 4)$  bytes before container  
882 compression. With  $N = 2 \cdot 10^5$  and  $d = 256$  the raw size is around fifty two megabytes. This  
883 removes any need to retain the full token matrix.884 D.7 Why pooling across tokens and not across channels  
885886 Spatial tokens form a redundant set of local descriptors that must be aggregated into a single global  
887 representation. Channel directions span a learned semantic basis. Averaging across channels pro-  
888 duces a length  $T$  vector that measures token magnitudes while discarding the basis geometry. In  
889 contrast averaging across tokens preserves the channel geometry and leads to a descriptor that aligns  
890 with downstream cosine retrieval. Formally consider a linear probe  $w \in \mathbb{R}^H$  that scores a semantic  
891 attribute. The pooled score from token pooling is  $w^\top m$  which equals the mean of per token scores  
892  $w^\top \tilde{V}_{\cdot \cdot}$ . Pooling across channels would instead collapse  $w$  into a scalar and break linear separability.  
893894 D.8 Pseudocode  
895896 **Algorithm 1** Step recording with compact descriptor  
897898 **Input** token features  $V \in \mathbb{R}^{T \times H}$ , image  $I$ , optional latent action  $A$  and discrete action ids  $g$ ; fixed  
899 projection  $P \in \mathbb{R}^{H \times d}$ .900 **Output** image file and feature file containing  $(q, s)$ , optional  $A, g$ .

- 901 1: normalize tokens row wise to obtain  $\tilde{V}$
- 902 2: compute  $m$  and  $x$  then  $u_0$  as in the equations above
- 903 3: compute  $u = \frac{u_0 P}{\|u_0 P\|_2 + \varepsilon}$
- 904 4: compute  $s = \max_j |u_j| / 127 + \delta$  and  $q = \text{round}(u/s)$
- 905 5: save  $I$  and a compressed archive with  $q$  as int8 and  $s$  as float32 and optional  $A, g$

907  
908 **Algorithm 2** Language conditioned similarity  
909910 **Input** two observations  $o_1, o_2$ , instruction  $L$ 911 **Output** similarity  $S \in [0, 1]$ 

- 912 1: dequantize stored summaries to obtain  $\hat{u}_1, \hat{u}_2$  and compute  $S_{\text{embed}}$
- 913 2: encode images and text to obtain  $z_1, z_2, t$  and compute  $S_{\text{clip}}, S_{\text{text}}$
- 914 3: if relation cues are enabled then detect gripper and target from  $L$ , compute  $r_1, r_2$  then  $S_{\text{rel}}$
- 915 4: combine into  $S_{\text{image}}$  using the weights  $\alpha_c, \alpha_t, \alpha_r$
- 916 5: if latent actions are present then compute  $S_{\text{act}}$
- 917 6: return fusion  $S$  using either additive or gated composition

918 **Pairwise similarity**  
919920 D.9 Recommended hyperparameters and practical notes  
921922 A projection dimension of two hundred fifty six offers a favorable accuracy storage tradeoff. The  
923 per vector quantizer with a single scale parameter is adequate for cosine based retrieval. The relation  
924 kernel uses standard deviations  $\sigma$  on the order of one third of typical variation for each component.  
925 The instruction gate uses the minimum of image text cosines which is robust to asymmetric matches.  
926 The random projection is sampled once and stored, which ensures reproducibility across runs.  
927928 D.10 Failure modes and mitigations  
929930 False positives can occur when appearance is similar but the instruction semantics differ. The instruc-  
931 tion gate and the relation kernel address this issue. Failure due to detector misses can be mitigated  
932 by falling back to the combination of image cosine and text gate. Duplicate frames can be forced  
933 to score near one through a gated fusion that preserves the coarse score, and through identity short  
934 circuits when identical summaries are detected numerically.  
935936 D.11 End to end retrieval  
937938 In large experience banks the proposed summary enables approximate nearest neighbor indexing.  
939 The query pipeline constructs the summary of the current frame, retrieves top candidates with  $S_{\text{embed}}$ ,  
940 then applies the reranker on that shortlist and returns the final ordering. This design preserves in-  
941 struction specificity while keeping the storage and time cost low.  
942943 E Failure Case Analysis  
944945 We investigated reinforcement learning for EFN using the SAC algorithm, where the reward was  
946 defined by the semantic similarity between the predicted next observation and the reference obser-  
947 vation sampled from the experience buffer. The Sinkhorn similarity metric was adopted to quantify  
948 semantic alignment in a high-dimensional embedding space. Despite its theoretical appeal, this de-  
949 sign exhibited several flaws that ultimately caused training failure.  
950951 First, the reward distribution was too narrow. Denote the raw similarity at step  $t$  as  
952

953 
$$R_t^{\text{raw}} = \text{SinkhornSim}(O_{t+1}, O_{t+1}^E), \quad (40)$$

954 where  $O_{t+1}$  is the predicted next embedding and  $O_{t+1}^E$  is the target embedding from the selected  
955 experience  $E$ . In practice,  $R_t^{\text{raw}}$  remained tightly clustered in  $[0.87, 0.93]$ . As a result, the critic  
956 received only weak gradients because the variance

957 
$$\text{Var}(R_t^{\text{raw}}) \approx 10^{-3} \quad (41)$$

958 was too small to differentiate between actions. To mitigate this, a normalization step was applied,  
959

960 
$$R_t^{\text{norm}} = \frac{R_t^{\text{raw}} - \mu_t}{\sigma_t}, \quad (42)$$

961 with running mean  $\mu_t$  and variance  $\sigma_t^2$ . However, because  $\mu_t$  was initialized near the empirical  
962 mean of the first batch, subsequent values of  $R_t^{\text{raw}}$  were often less than  $\mu_t$ , producing predominantly  
963 negative  $R_t^{\text{norm}}$ . This inversion of sign transformed the optimization objective from maximizing pos-  
964 itive returns to minimizing cumulative penalties, leading to unstable critic estimates and oscillatory  
965 Q-values.  
966967 Second, the target of imitation changed inconsistently across steps. At each time  $t$ , the experience  
968 trajectory  $E$  was reselected to maximize semantic alignment with the current observation. This  
969 meant that the optimization target  
970

971 
$$\min_{\pi} \mathbb{E} \left[ \|f(O_{t+1}) - f(O_{t+1}^E)\|^2 \right] \quad (43)$$

972 was computed against a moving reference  $O_{t+1}^E$  that varied with  $t$ . Frequent switching between  
973 different trajectories undermined the stationarity assumption of reinforcement learning and prevented  
974

972 the critic from converging toward a consistent value function. The instability was exacerbated by  
 973 the replay buffer, which stored transitions associated with outdated experience selections, further  
 974 degrading learning.

975 Third, the scale of the embedding space posed intrinsic difficulties. Each observation embedding  
 976 was represented as a tensor  
 977

$$O_t \in \mathbb{R}^{256 \times 4096}, \quad (44)$$

979 and the latent action correction operated in the space  
 980

$$\Delta A_t \in \mathbb{R}^{4 \times 4096}. \quad (45)$$

982 The dimensionality of these matrices is extremely high, with each step involving more than one  
 983 million parameters in the observation representation alone. This created an environment where the  
 984 actor–critic updates were easily overwhelmed by noise and variance, making exploration highly  
 985 inefficient. SAC, which relies on accurate Q-function estimation, struggled to propagate meaningful  
 986 gradients in such a vast search space.

987 In summary, the failure arose from a combination of (i) overly concentrated similarity-based re-  
 988 wards that became negative after normalization, (ii) non-stationary targets caused by continuous  
 989 switching between different experience trajectories, and (iii) the excessive dimensionality of the em-  
 990 bedding and action spaces that rendered stable credit assignment infeasible. This case highlights  
 991 that reinforcement learning with high-dimensional semantic rewards requires careful reward shap-  
 992 ing, fixed reference trajectories, and dimensionality reduction strategies in order to achieve stable  
 993 convergence.

## 995 F Token-level Entropic Optimal Transport for `SINKHORN_SIMILARITY`

998 **Setting.** Let  $X \in \mathbb{R}^{T_x \times D}$  and  $Y \in \mathbb{R}^{T_y \times D}$  denote token embeddings for two observations, with  
 999 feature dimension  $D$  and token counts  $T_x$  and  $T_y$ . In our experiments  $T_x = T_y = 256$  and  $D = 4096$ ,  
 1000 while the derivation is general. The objective is to measure fine-grained agreement between  $X$  and  
 1001  $Y$  without spatial pooling by aligning tokens through an entropic optimal transport plan.

1002 **Cosine affinity.** Each token is  $\ell_2$ -normalized along the feature dimension with a small numerical  
 1003 constant  $\varepsilon_n > 0$ :

$$\hat{X}_{i \cdot} = \frac{X_{i \cdot}}{\|X_{i \cdot}\|_2 + \varepsilon_n}, \quad \hat{Y}_{j \cdot} = \frac{Y_{j \cdot}}{\|Y_{j \cdot}\|_2 + \varepsilon_n}. \quad (46)$$

1007 The token-by-token cosine affinity is  
 1008

$$S = \hat{X} \hat{Y}^\top \in [-1, 1]^{T_x \times T_y}, \quad S_{ij} = \langle \hat{X}_{i \cdot}, \hat{Y}_{j \cdot} \rangle. \quad (47)$$

1011 **Entropic OT objective.** Set  $C = -S$  so that larger similarity yields smaller cost. With uniform  
 1012 marginals

$$r = \frac{1}{T_x} \mathbf{1}_{T_x}, \quad c = \frac{1}{T_y} \mathbf{1}_{T_y}, \quad (48)$$

1015 the balanced entropic OT problem reads  
 1016

$$\min_{P \in \mathbb{R}_{\geq 0}^{T_x \times T_y}} \langle P, C \rangle - \varepsilon H(P) \quad \text{subject to} \quad P \mathbf{1}_{T_y} = r, \quad P^\top \mathbf{1}_{T_x} = c, \quad (49)$$

1019 where  $\varepsilon > 0$  controls the entropic regularization and  
 1020

$$H(P) = - \sum_{i=1}^{T_x} \sum_{j=1}^{T_y} P_{ij} (\log P_{ij} - 1) \quad (50)$$

1024 is the Shannon entropy. The entropy makes the problem strictly convex and yields a strictly positive  
 1025 solution.

1026 **Gibbs kernel and Sinkhorn–Knopp scaling.** The optimal solution admits the factorization  
 1027

$$1028 \quad P^* = \text{diag}(u) K \text{ diag}(v), \quad K = \exp\left(\frac{S}{\varepsilon}\right), \quad (51)$$

1030 for unique scaling vectors  $u \in \mathbb{R}_{>0}^{T_x}$  and  $v \in \mathbb{R}_{>0}^{T_y}$  that match the marginals. They are obtained by  
 1031 the fixed-point updates

$$1032 \quad u^{(t+1)} = r \oslash (K v^{(t)} + \delta), \quad (52)$$

$$1033 \quad v^{(t+1)} = c \oslash (K^\top u^{(t+1)} + \delta),$$

1034 where  $\delta > 0$  stabilizes divisions and  $\oslash$  denotes elementwise division. For strictly positive  $K$  the  
 1035 iterations converge geometrically to the unique scaling pair.

1037 **Similarity score and reward mapping.** The raw alignment value is the inner product between the  
 1038 transport plan and the affinity:

$$1040 \quad \text{score} = \langle P^*, S \rangle = \sum_{i=1}^{T_x} \sum_{j=1}^{T_y} P_{ij}^* S_{ij}. \quad (53)$$

1043 Under uniform marginals one has

$$1044 \quad \sum_{i=1}^{T_x} \sum_{j=1}^{T_y} P_{ij}^* = \mathbf{1}_{T_x}^\top P^* \mathbf{1}_{T_y} = \mathbf{1}_{T_x}^\top r = 1, \quad (54)$$

1047 hence  $\text{score} \in [-1, 1]$  because  $S_{ij} \in [-1, 1]$ . For reinforcement learning the value is mapped to  
 1048  $[0, 1]$  as

$$1049 \quad \text{score}_{01} = \frac{1}{2}(\text{clip}(\text{score}, -1, 1) + 1). \quad (55)$$

---

1051 **Algorithm 3** `sinkhorn_similarity` ( $X, Y; \varepsilon, n_{\text{iters}}$ )

---

1053 1:  $\hat{X} \leftarrow \text{row-normalize}(X)$ ,  $\hat{Y} \leftarrow \text{row-normalize}(Y)$   
 1054 2:  $S \leftarrow \hat{X} \hat{Y}^\top$ ,  $K \leftarrow \exp(S/\varepsilon)$   
 1055 3:  $r \leftarrow \frac{1}{T_x} \mathbf{1}_{T_x}$ ,  $c \leftarrow \frac{1}{T_y} \mathbf{1}_{T_y}$   
 1056 4:  $u \leftarrow \mathbf{1}_{T_x}$ ,  $v \leftarrow \mathbf{1}_{T_y}$   
 1057 5: **for**  $t = 1$  to  $n_{\text{iters}}$  **do**  
 1058 6:    $u \leftarrow r \oslash (K v + \delta)$   
 1059 7:    $v \leftarrow c \oslash (K^\top u + \delta)$   
 1060 8: **end for**  
 1061 9:  $P \leftarrow \text{diag}(u) K \text{ diag}(v)$   
 1062 10:  $\text{score} \leftarrow \langle P, S \rangle$   
 1063 11:  $\text{score}_{01} \leftarrow \frac{1}{2}(\text{clip}(\text{score}, -1, 1) + 1)$   
 1064 12: **return**  $\text{score}_{01}, P, S$

---

1066 **Role of the temperature.** The parameter  $\varepsilon$  governs the sharpness of the kernel. When  $\varepsilon$  is small  
 1067 the kernel concentrates mass on pairs with large cosine similarity and the solution approaches a soft  
 1068 permutation that emphasizes near one-to-one matches. When  $\varepsilon$  is large the plan spreads mass more  
 1069 diffusely and gradients become smoother. Empirically a range between 0.03 and 0.1 performs well  
 1070 for  $T_x = T_y = 256$ .

1072 **Differentiability.** The map from  $(X, Y)$  to  $S$  is smooth after row normalization, the exponential  
 1073 kernel is smooth, and the Sinkhorn updates consist of matrix–vector products and stable elementwise  
 1074 operations. Gradients can be backpropagated through  $u$  and  $v$  into  $K$  and  $S$ , and finally into  $X$  and  
 1075  $Y$ . If desired, the clipping in  $\text{score}_{01}$  can be replaced by a smooth squashing such as a logistic  
 1076 function to avoid saturation.

1077 **Complexity and memory.** For  $T_x = T_y = T$ , the kernel construction and each Sinkhorn iteration  
 1078 cost  $O(T^2)$  time and  $O(T^2)$  memory. With  $T = 256$  the matrices contain 65,536 entries, which is  
 1079 tractable on modern accelerators even with multiple iterations.

1080  
 1081 **Numerical stabilization.** Underflow and overflow can arise when  $\varepsilon$  is very small. A common  
 1082 remedy is recentering before exponentiation:  
 1083

$$1084 \quad K = \exp\left(\frac{S - \max(S)}{\varepsilon}\right), \quad (56)$$

1085 which leaves the optimal  $P^*$  unchanged up to rescaling of  $u$  and  $v$  because the Sinkhorn scaling  
 1086 absorbs global factors. The constant  $\delta$  in the updates prevents division by zero in transiently sparse  
 1087 rows and columns.  
 1088

1089 **Relation to exact matching.** Let  $\Pi(r, c)$  denote the transport polytope with the given marginals.  
 1090 In the limit  $\varepsilon \rightarrow 0$  one recovers the linear assignment problem  
 1091

$$1092 \quad \arg \min_{P \in \Pi(r, c)} \langle P, -S \rangle, \quad (57)$$

1093 whose solution becomes a permutation matrix when  $T_x = T_y$  and the optimum is unique. The  
 1094 entropic formulation therefore interpolates between hard assignment and a smooth strongly convex  
 1095 surrogate that is well suited to gradient-based learning.  
 1096

1097 **Reward semantics in EFN.** The value score<sub>01</sub> quantifies token-accurate agreement between the  
 1098 predicted next observation and the target derived from the retrieved experience. Because mass can  
 1099 be distributed across multiple token correspondences according to their cosine affinity, the signal  
 1100 remains informative when only parts of the scene follow the intended dynamics, which reduces  
 1101 reward sparsity compared with global image pooling.  
 1102

1103 **Generalizations.** Occlusions and appearance changes can be modeled by relaxing the marginal  
 1104 constraints with Kullback–Leibler penalties, leading to the unbalanced objective  
 1105

$$1106 \quad \min_{P \geq 0} \langle P, C \rangle - \varepsilon H(P) + \tau_r \text{KL}(P \mathbf{1}_{T_y} \| r) + \tau_c \text{KL}(P^\top \mathbf{1}_{T_x} \| c), \quad (58)$$

1107 which is compatible with generalized Sinkhorn updates. Nonuniform marginals can encode spatial  
 1108 priors by reweighting  $r$  and  $c$ .  
 1109

1110  
 1111  
 1112  
 1113  
 1114  
 1115  
 1116  
 1117  
 1118  
 1119  
 1120  
 1121  
 1122  
 1123  
 1124  
 1125  
 1126  
 1127  
 1128  
 1129  
 1130  
 1131  
 1132  
 1133